ADVANCED FUNCTIONAL MATERIALS
www.afm-journal.de

Biomimetic Approach for Sustainable Magnetite Nanoparticle Synthesis Using Polycations

Lucas Kuhrts, Sylvain Prévost, Ernesto Scoppola, Ann-Marie Hirt, and Damien Faivre**

Magnetotactic bacteria produce magnetite nanoparticles called magnetosomes at ambient conditions via a protein-stabilized transient amorphous precursor to obtain precise control over particle size and morphology. In a bioinspired approach, such biomineralization processes are emulated, mimicking proteins involved in magnetosome formation using the positively charged analog poly-L-arginine. While the additive is expensive, it remains elusive whether the change in magnetite formation mechanism arises solely from the polymer's cationic nature. This study uses different mass-produced and sustainably sourced polycations to induce the biomineralization-reminiscent formation of magnetite nanoparticles. These findings present how to achieve control over nanoparticle size (from 10 to 159 nm) and morphology (compact and sub-structured) as well as magnetic properties (superparamagnetic, stable-single-domain, vortex state) at ambient temperature and pressure using these additives. Furthermore, the formation of large nanoparticles with the addition of poly(diallyldimethylammonium chloride) (PDADMAC) at low alkalinity highlights how magnetotactic bacteria may produce magnetite nanoparticles under similar conditions. Confirming the polycations' ability to electrostatic stabilize amorphous ferrihydrite, it is anticipated that parametric in vitro studies on polymer properties will provide valuable insights into magnetite biomineralization and aid in rationally designing magnetic nanomaterials.

1. Introduction

Magnetite (Fe_3O_4), the naturally most abundant magnetic iron ore, is encountered in geologic and biomineralizing systems, as well as in various man-made applications.[1,2] Tailoring magnetite magnetic properties is achieved by synthetically controlling nanoparticles' shape, texture, organization, purity,[3–5] and most importantly its dimension. Magnetite nanoparticles exhibit superparamagnetism below and ferrimagnetic properties above the size threshold of 20 nm.[6,7] Thus, rationally designing the size of the nanoparticles will permit a fine-tuning of their properties toward their versatile applications ranging from water purification,[8] ink materials,[9] magnetic data storage,[10] or ferrofluids[11] to biomedical application such as contrast agents in magnetic resonance imaging (MRI) and in hyperthermia therapy in cancer treatment.[12,13] While hot-injection methods using organic solvents and additives have set a benchmark in magnetite nanoparticle size control,[14,15] achieving similar control is notoriously difficult outside unsustainable conditions.[16] Aqueous routes such as the coprecipitation technique of ferrous and ferric iron at increased alkalinity, the industrially most relevant process for the production of magnetite, only produce agglomerated, polydisperse particles.[2,17,18]

Biomineralization's distinguishing characteristic is the ability to nucleate crystals of complex shape in an aqueous environment at ambient conditions by employing transient amorphous precursors.[19–22] These precursors are kinetically favored over their thermodynamically more stable final crystalline phase and transform to such, via densification and dehydration in a cascade-like fashion.[23] The kinetics of these transformations are highly dependent on the presence of macromolecular and/or ionic additives, giving the possibility to alter the crystallization energy landscape to influence product morphology, size, and texture.[24–28] Naturally occurring magnetite is formed by a number of species including bees, migratory birds, and fish for its magnetic properties,[29] while others produce magnetite for its superior hardness.[30] The latter is exploited by chitons, a marine mollusk that feeds off rock-attached algae, which control magnetite formation via ferrihydrite using acidic macromolecules.[31]

L. Kuhrts, E. Scoppola, D. Faivre
Max Planck Institute of Colloids and Interfaces
Department of Biomaterials
Am Mühlenberg 1, 14476 Potsdam, Germany
E-mail: lucas.kuhrts@campus.technion.ac.il; damien.faivre@cea.fr
S. Prévost
Institut Laue-Langevin – The European Neutron Source
71 avenue des Martyrs, CS 20156, Grenoble Cedex 9 38042, France
A.-M. Hirt
ETH Zürich Dep. of Earth Science
Sonneggstrasse 5, Zürich 8092, Switzerland
D. Faivre
Aix-Marseille University, CNRS, CEA, BIAM
Saint-Paul-lez-Durance 13115, France

The ORCID identification number(s) for the author(s) of this article can be found under https://doi.org/10.1002/adfm.202311856

DOI: 10.1002/adfm.202311856

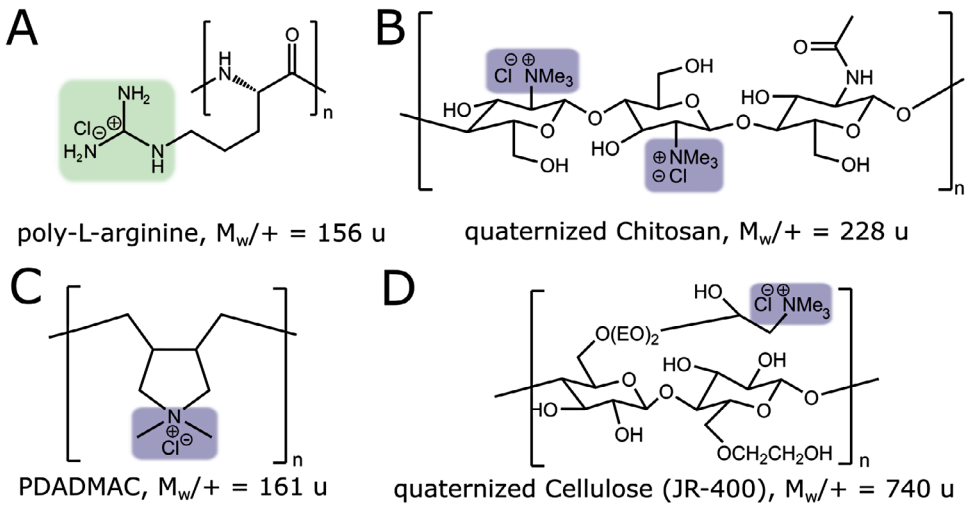

Figure 1. Strong polycations used in this study with corresponding molecular mass per positive charge. Guanidino group (green) is positively charged at all pH values investigated in this study, while quaternary amines (blue) are positively charged at any pH.

Most prominently, magnetotactic bacteria form ferrimagnetic magnetite nanoparticles of precisely defined size and shape, unmatched by present synthetic protocols, from disordered ferrihydrite-like ferritin at ambient conditions.[32] Mimicking such processes in vitro, to achieve similar sophistication in magnetite formation as showcased in biomineralizing systems, has been the objective of numerous recent publications.[16,33–35]

Alternative bioinspired magnetite synthesis focused on the addition of proteins,[35,36] and other charged macromolecules, using classical coprecipitation reactions, as well as ammonia diffusion coprecipitation and partial oxidation of ferrous hydroxides.[33,37-39] An approach close to the natural system is the formation of magnetite nanoparticles using magnetite biomineralization-associated proteins,[36] recombinantly produced in *E. coli* and consequently added to the synthesis of magnetite, resulting, e.g., in an increase in particle size and a change of nanoparticle morphology.[35,40] For the larger-scale production of such nanoparticles, the applicability of proteins is hampered by their time-consuming and costly synthesis, concomitant with a low material yield. We thus extended the protein-based strategy to the use of an homopolyelectrolyte as a synthetic protein analog: poly-L-arginine.[41] By using this positively charged polycation, the control over size, size distribution, morphology, and colloidal stability was significantly improved.[42,43] Furthermore, this was considered to be a direct result of a biomineralization-resembling formation mechanism induced by the addition of poly-L-arginine.[28] However, it remains elusive whether complementary reaction pathways inducing similarly advanced control on nanoparticle morphology can be achieved by the addition of generic polycations. Here, we present the effect of strong polycations (**Figure 1**) — charged independently of pH — on the co-precipitation of ferrous and ferric chloride at alkaline conditions. Whereas previous research relied on the use of difficult-to-synthesize proteins and rather expensive protein analogs in the production of magnetite nanoparticles, we strive to increase the sustainability and economics of the synthesis by the addition of inexpensive polycations or positively charged sugar-based polymers from renewable sources. Therefore, quaternized chitosan, sourced from shrimp waste, and JR-400, an industrially, metric tons-scale produced cellulose-based polycation, which is used in shampoos and lotions, andPDADMAC, a laboratory abundant and inexpensive strong polycation, are tested as additives in the synthesis of magnetite nanoparticles. We show that all the tested polycations induce a similar crystallization pathway in magnetite as the one induced by poly-L-arginine resembling that of magnetite biomineralization. This enables us to obtain excellent control over nanoparticle size, morphology, and magnetic properties, using sustainably sourced polycations.

2. Results

Magnetite nanoparticles were co-precipitated from 0.1 M ferrous (Fe^{2+}) and ferric (Fe^{3+}) chloride solution (molar ratio 1:2) in aqueous sodium hydroxide, corresponding to the protocol used by Kuhrts et al.[42] We used a computer-controlled setup that regulates the flux of the iron solution at 1 µL min^{-1}, while a pH-electrode-connected titration device kept a constant pH. Magnetite nanoparticles were grown for 2 h at pH 9, 10, and 11 in the presence of 0.1 mg mL^{-1} poly-L-arginine as a reference,[42] and compared to nanoparticles grown under the same conditions with strong polycations quaternized chitosan (chitosan), polydiallyldimethylammonium chloride (PDADMAC), or quaternized cellulose (JR-400) as additives. The formed magnetite nanoparticles were imaged using transmission electron microscopy (TEM) shown in **Figure 2** to determine nanoparticle morphology. While nanoparticles prepared in the presence of poly-L-arginine, JR-400, and chitosan appear as compact single-crystals at pH 9 and 10, at pH 11 a sub-structuring arises under retention of their single-crystalline nature evident from the Fast Fourier Transform (FFT) of corresponding high resolution (HR)TEM images (images left of low magnification pH 11 nanoparticles in Figure 2). However, this change in morphology at pH 11 is not observed for nanoparticles prepared in the presence of PDADMAC, which remain compact nanoparticles for all pH values tested. Comparing magnetite nanoparticles prepared in the presence of all polycationic additives to the coarse-grained control nanoparticles (see

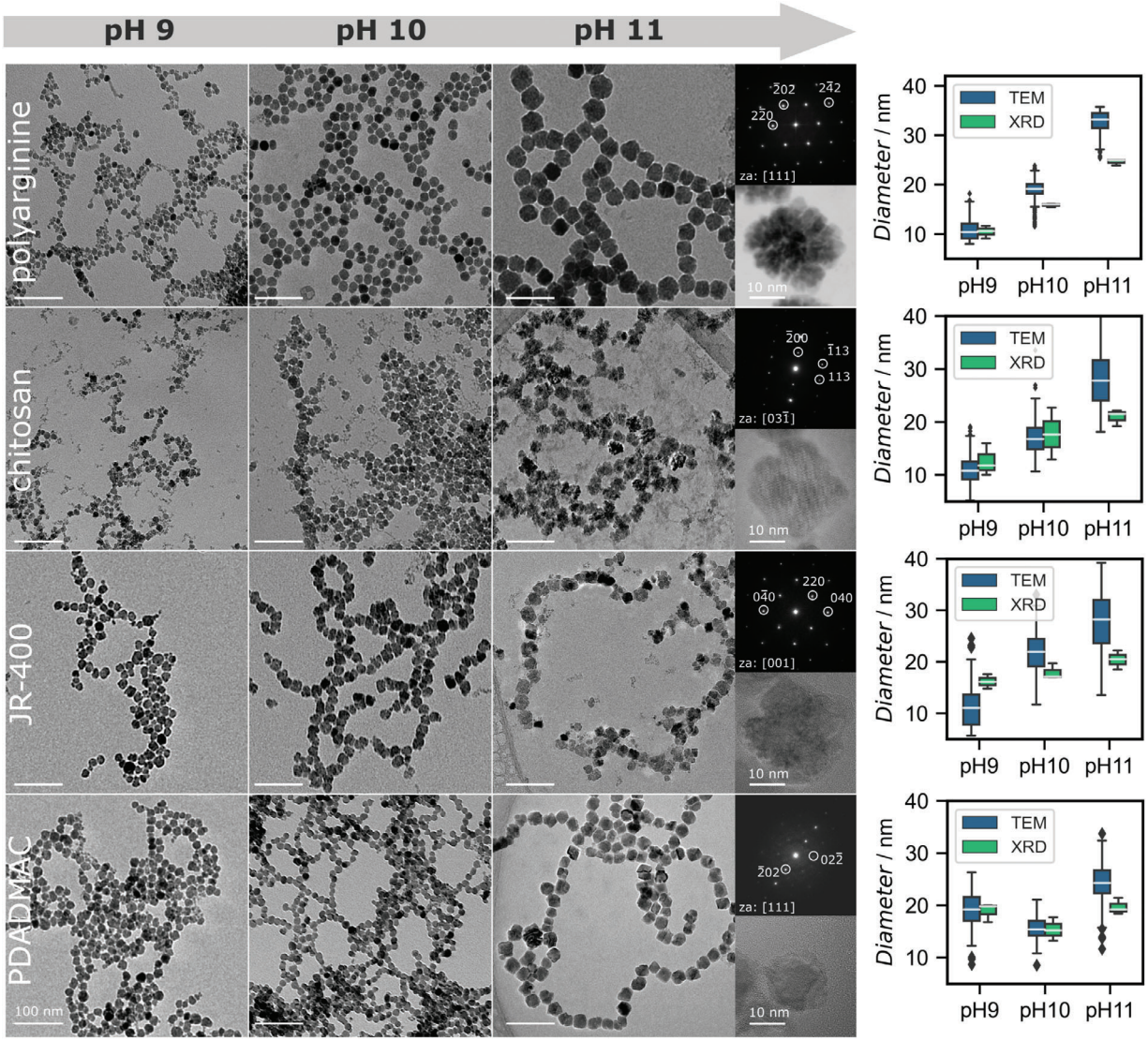

Figure 2. TEM micrographs of magnetite nanoparticles prepared in the presence of poly-L-arginine, quaternized chitosan, JR-400, and PDADMAC (top to bottom) at pH 9, 10, and 11 (left to right). High-resolution contrast-inverted HAADF STEM for poly-L-arginine and high-resolution TEM micrographs for nanoparticles prepared at pH 11 with corresponding FFTs are shown to the right of the low-magnification images. A clear sub-structuring with retention of single-crystallinity, as indicated by the FFTs, is visible for particles prepared in the presence of poly-L-arginine, chitosan, and JR-400, while solid, single-crystalline particles are obtained in the presence of PDADMAC at pH 11. Particle sizes obtained from Scherrer analysis of the (311) PXRD reflections for all pH are given in the right column with error bars calculated from experimental triplicates. Sizes calculated for TEM represent particle size distribution within a population of at least 150 nanoparticles measured in one sample. The upper and lower borders of the box represent the upper and lower quartile, respectively. Scale bar for low magnification TEM is 100 nm and for high magnification TEM 10 nm.

Figure S1, Supporting Information), it is evident that the addition of strong polycations induces the formation of well shape-defined globular nanoparticles. Furthermore, the colloidal stability of the nanoparticles is drastically increased due to the adsorption of polycations, inducing electrostatic (zeta potential = 29 mV) and steric stabilization and preventing nanoparticle aggregation across all sizes produced here (see Figure S2, Supporting Information).

Average nanoparticle sizes from synthesis triplicates, shown in Figure 2 and summarized in **Table 1**, are determined from synchrotron powder X-ray diffraction (PXRD) using the Scherrer equation[44] on the peak broadening of the (220), (311), (400), (422), (511), and (440) magnetite reflection (see Figures S3–S7, Supporting Information). As there is no significant deviation of nanoparticle sizes calculated within the ensemble of reflection, we use the nanoparticle sizes calculated from the most intense magnetite (311) reflection, to represent the distribution of particle sizes obtained in triplicated synthesis. At increased alkalinity, larger nanoparticles form with sizes ranging from 10 to 25 nm for poly-L-arginine and from 12 to 23 nm for quaternized chitosan and JR-400. PDADMAC does not exhibit a direct proportionality of nanoparticle size with pH, resulting in nanoparticle sizes of 20, 18, and 23 nm for pH 9, 10, and 11, respectively. Most importantly, unlike additive-free magnetite nanoparticles

Table 1. Mean particles diameters at different pH analyzed by TEM and XRPD.

Polymer	pH	Syn. Time [h]	D_{XRPD} [nm]	D_{TEM} [nm]	H_C [mT]	a [Å]	lattice distance [%]
poly-L-arginine	9	2	10 ± 1.4	9 ± 1.9	-	8.358(6)	-0.45
	10	2	16 ± 0.4	18 ± 1.3	-	8.376(7)	-0.24
	11	2	24 ± 0.5	32 ± 1.9	6.9	8.376(7)	-0.23
chitosan	9	2	11 ± 0.8	10 ± 2	-	8.359(5)	-0.43
	10	2	18 ± 2.4	16 ± 2.6	-	8.371(3)	-0.29
	11	2	19 ± 0.8	27 ± 6.1	0.1	8.357(7)	-0.46
JR-400	9	2	16 ± 1.5	10 ± 3.9	-	8.376(6)	-0.23
	10	2	17 ± 1.7	21 ± 4.1	-	8.376(3)	-0.24
	11	2	21 ± 1.8	27 ± 5.2	11.9	8.382(2)	-0.17
PDADMAC	9	2	18 ± 1.5	18 ± 3.6	-	8.358(6)	-0.26
	10	2	15 ± 2.3	15 ± 2.5	-	8.376(3)	-0.34
	11	2	18 ± 0.8	22 ± 4.1	3.2	8.376(7)	-0.23
poly-L-arginine	11	24	40.7	102±15	16.4	8.407(6)	+0.13
chitosan	11	24	32.2	85±22	16.0	8.410(7)	+0.16
JR-400	11	24	20	88±30	25.6	8.401(1)	+0.05
PDADMAC	11	24	27.5	59±7	33.8	8.391(4)	-0.06

Particles size distributions from TEM were calculated from single particles in an ensemble of at least 150 particles, while for XRPD mean particle sizes were calculated from triplicates. Vibrating sample magnetometry (VSM) was used to calculate coercivities (H_C) for selected samples. Lattice parameter a = b = c of the magnetite cubic crystal lattice are determined from averaging lattice constants calculated for (220), (311), (400), (422), (511), and (440) magnetite reflection and lattice distortions calculated in percent using the lattice spacing of 8.3965 Å of compositionally pure magnetite. Errors for size determination are calculated from the standard deviation of the Gauss distribution, while errors given in parenthesis indicate uncertainties in the measurement.

(see Figure S1D, Supporting Information), we find an inversion of the final nanoparticle size as a function of pH. While pure magnetite nanoparticles exhibit smaller sizes with an increased pH, the opposite is observed upon the addition of polycations, where the final nanoparticle sizes increase with pH. The full PXRD patterns, shown in Figures S3–S6 (Supporting Information), can be indexed according to the inverse spinel structure of magnetite. From the peak position of the reflection (311), we calculate the lattice parameter a = b = c of the cubic system, shown in Table 1, ranging from a minimum $d_{(100)}$-spacing of 8.3688 Å(0.33% lattice compression) to a maximum of 8.3795 Å(0.2% lattice compression) indicating slight surface oxidation in all samples common to nanoscopic magnetite, resulting in a decrease in the lattice parameter from compositionally pure magnetite (8.3965 Å).

We confirm the nanoparticle size trend in dependence of synthesis pH observed in PXRD using nanoparticle size analysis based on TEM images of at least 150 nanoparticles, giving nanoparticle sizes ranging from 9 ± 2 to 33 ± 2 nm for poly-L-arginine, 10 ± 2 to 27 ± 5 nm for quaternized chitosan, 10 ± 4 to 28 ± 6 nm for JR-400, and from 18 ± 3 to 23 ± 4 nm for PDADMAC (see Figure S16, Supporting Information). From a linear fit of the particle size dependence on pH, we obtain 12.5 nm pH^{-1} for poly-L-arginine, around 8.5 nm pH^{-1} for JR-400 and chitosan, while nanoparticles formed in the presence of PDADMAC do not show a clear linear pH dependence. Using TEM further allows for the determination of the intrinsic size distribution of a population in one sample shown in Figure 2, summarized in Table 1, indicating a narrow size distribution for all polycations tested, compared to the additive-free magnetite sample (see Figure S1, Supporting Information), whose large intrinsic size distribution can only qualitatively determined, due to a strong agglomeration and overlap of the nanoparticles. The deviation from nanoparticle sizes when comparing XRD and TEM, especially from nanoparticles prepared at pH 11, can arise from the occasionally observed twinning (see Figure S17, Supporting Information) in some magnetite nanoparticles. These twins are crystallographically not coherent and appear as two separate nanoparticles in XRD, while in TEM they appear as one solid nanoparticle.

Our previous study[28] demonstrated that the growth of magnetite nanoparticles in the presence of poly-L-arginine is interrupted when reaching a chloride concentration of 10 mM released in the reaction of $FeCl_2$ and $FeCl_3$ screening the charges of poly-L-arginine and depressing the interaction with the growing magnetite. This poisoning effect of chloride can be overcome by increasing the reaction volume to 60 mL and keeping the addition rate of iron at 1 µL min^{-1}. This increases the growth time until the threshold chloride concentration reaches 24 h. Testing this approach at pH 11 for the presented polycations, we obtain magnetite nanoparticles with maximum sizes of up to 107 nm for poly -L -arginine, 112 nm for chitosan, 159 nm for JR-400, and 84 nm for PDADMAC, shown in TEM images in **Figure 3**. For these large nanoparticles, the morphology is even better visible, observing sub-structured, spherical nanoparticles with a rough interface in the case of poly-L-arginine, chitosan, and JR-400. In contrast, for PDADMAC solid, faceted nanoparticles are obtained likely exhibiting a cuboctahedral 3D shape with a triangular (111) face within the image plane. All nanoparticles show selected area electron diffraction of single crystals independent of the morphology of the nanoparticle (Figure 3). Using PXRD, we calculate average lattice parameter from the peak positions of the (220), (311), (400), (422), (511), and (440) magnetite reflection for the large nanoparticles, which lie consistently above the lattice parameters reported for nanoparticles grown for 2 h (see Figure SI 10, Supporting Information). Whereas the latter nanoparticles show $d_{(100)}$-spacings of 8.3688 – 8.3795Å, the large nanoparticles exhibit lattice spacings of 8.4071 Å (0.13% lattice expansion) for poly-L-arginine, 8.4104 Å (0.16% lattice expansion) for chitosan, 8.4013 Å (0.05% lattice expansion) for JR-400, and 8.391 Å (0.06% lattice compression) for PDADMAC indicating a lower relative contribution of an oxide surface layer, consistent with a lower surface to volume ratio of large nanoparticles.[45] The lattice expansion for poly-L-arginine, JR-400, and chitosan may arise from physical gaps within the sub-structured "single-crystalline" nanoparticles or indicate incorporation of the organic polymer into the crystal lattice of magnetite, which can result in crystal lattice expansion.[46,47] Our ability to grow such large nanoparticles provides further evidence for the previously reported[28] monomer attachment mechanism by which magnetite grows in the presence of polycations so that a quasi-infinite nanoparticle growth can be achieved.

The reminiscence of the poly-L-arginine-based formation mechanism to what is observed in magnetotactic bacteria was elucidated based on the growth mechanism determined from smallangle X-ray scattering (SAXS) measurements in situ.[28]

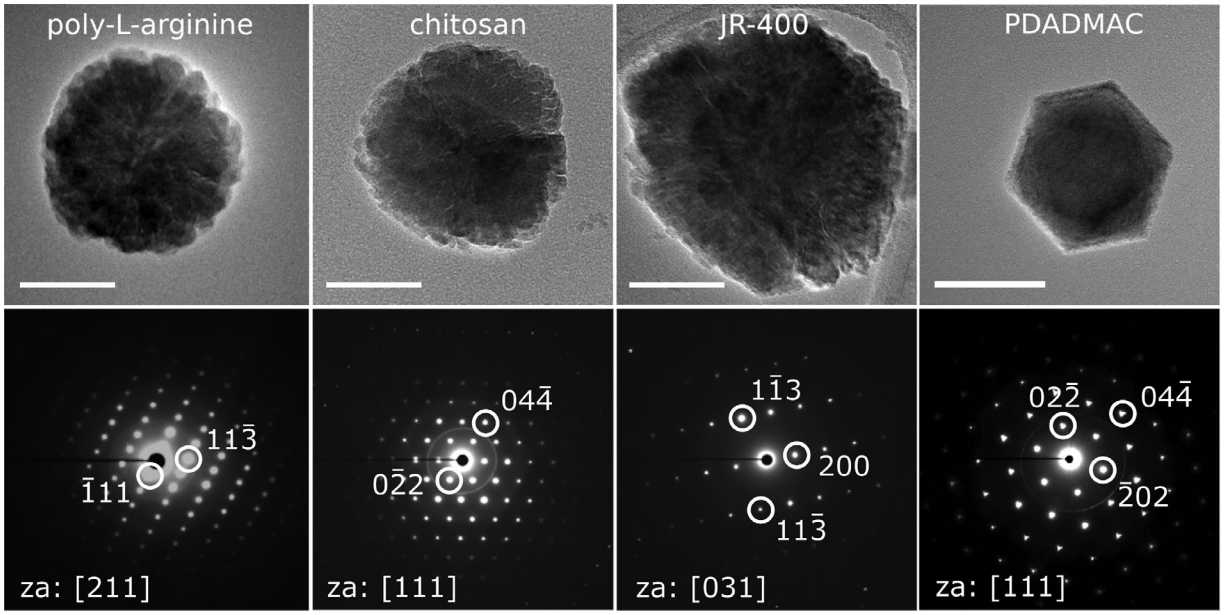

Figure 3. TEM micrographs of magnetite nanoparticles grown in the presence of different polycations for 24 h at pH 11. Corresponding selected area electron diffraction patterns, indexed according to the spinel crystal structure of magnetite are shown, indicating single-crystallinity for all nanoparticles. The difference between sub-structured nanoparticles grown in the presence of poly-L-arginine, chitosan, and JR-400 and solid nanoparticles grown in the presence of PDADMAC is well visible. Scale bars 50 nm.

Analogously to the in situ SAXS measurements, we determined the magnetite growth mechanism in the presence of selected polycations using PXRD, taking hourly aliquots during nanoparticle synthesis using the adapted protocol for extended growth. Nanoparticle sizes were calculated from the average sizes obtained from the (220), (311), (400), (422), (511), and (440) reflection using the Scherrer equation for selected pHs and polycations shown in **Figure 4**. We fitted the nanoparticle growth using a generic growth law as $R(t) = kt^{\frac{1}{\alpha}}$, where α is the growth exponent, indicative of the nanoparticle formation mechanism and k the growth rate. From a global fitting of the growth exponent for JR-400 and chitosan, we obtain α of 4.2, while magnetite nanoparticles obtained in the presence of PDADMAC at pH 10 deviate exhibiting a growth exponent of 2.6. These values lie above the growth exponent found for pure magnetite ($\alpha = 1$)[41] indicating a slowing-down of the reaction mechanism upon addition of the polycations, similar to what was observed for poly-L-arginine ($\alpha = 2.6$) further underlining the generality of magnetite formation in the presence of polycations compared to additive-free magnetite. Using vibrating sample magnetometry (VSM) the magnetic response to an externally applied magnetic field of magnetite nanoparticles grown for 2 h at pH 11 in the presence of different polymers is determined. **Figure 5A** shows an open hysteresis loop for all samples, except chitosan, indicating the presence of stable single domain (SSD) nanoparticles (H_C>0) with coercivities of 11.9 mT for JR-400, 6.9 mT for poly-L-arginine, and 3.2 mT for PDADMAC. The chitosan sample shows a wasp-waisted loop, suggesting the additional presence of nanoparticles with a diameter smaller than 22 nm giving a superparamagnetic (SP) response ($H_C = 0$) and nanoparticles with a coercivity of 1.3 mT.

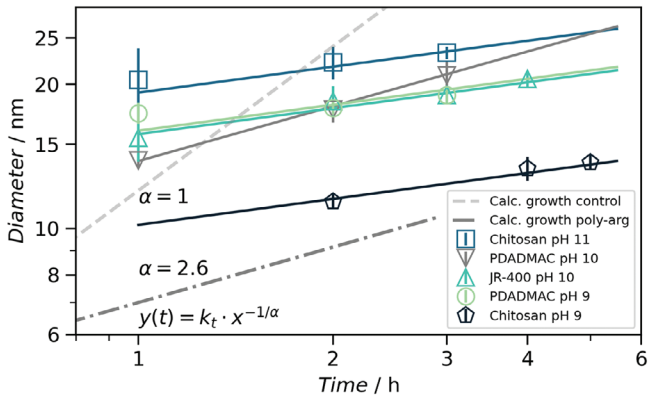

Figure 4. Time-dependent nanoparticle sizes at different pH for all polycations at selected pH obtained from PXRD. Error bars were calculated from standard deviation of the mean of nanoparticle sizes obtained from the (220), (311), (400), (422), (511), and (440) reflection. The growth exponent ($\alpha = 4.2$) was globally fitted to the growth of magnetite nanoparticles in the presence of JR-400, chitosan, and PDADMAC at pH 9. PDADMAC grown at pH 10 deviated, exhibiting a growth exponent of 2.6. All growth exponents thus lie above the growth exponent for additive-free magnetite ($\alpha = 1$)[17] similar to what is observed for poly-L-arginine ($\alpha = 2.6$).[28]

For large nanoparticles grown for 24 h, the magnetic response is more complex due to a broader size distribution. We thus determine the magnetic properties from first-order reversal curves (FORC) to obtain a more detailed characterization of the magnetic interactions and domain behavior in the samples. The FORC diagrams, shown in Figure 5B–E, depicting the coercivity field (B_C) along the abscissa and the magnetic interaction field (B_U) along the ordinate, show three features inherent to all samples. N.B., B_C relates to the coercivity spectrum of the magnetic

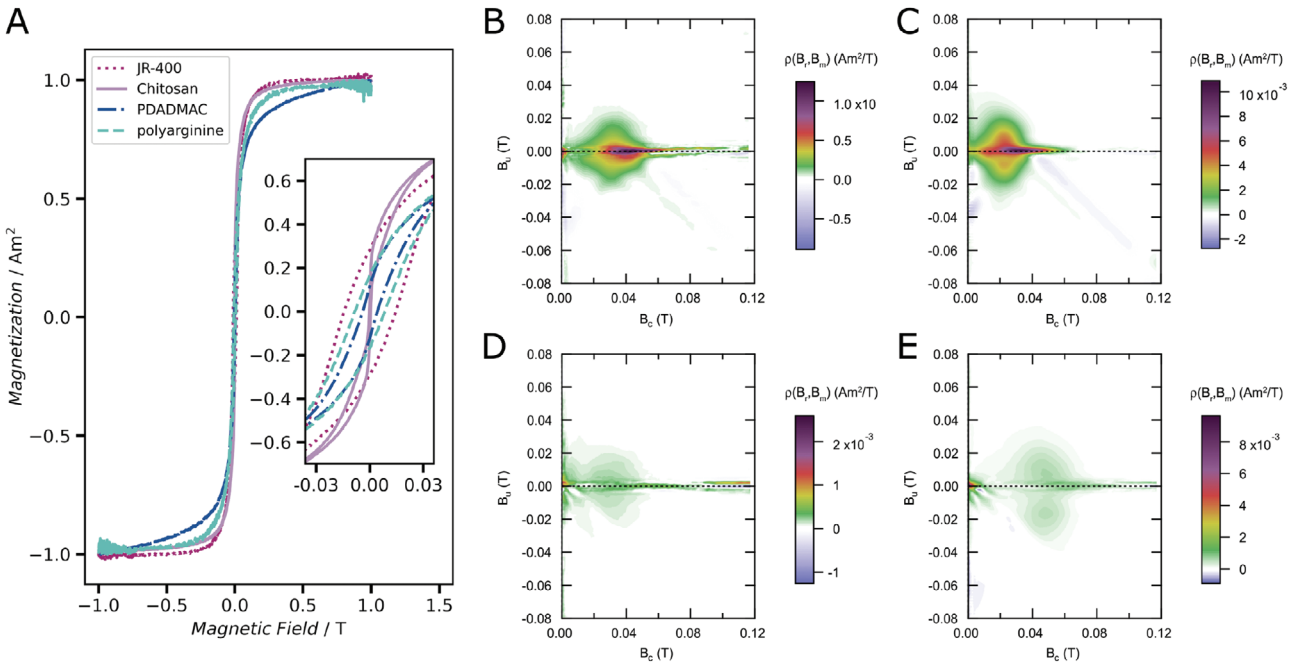

Figure 5. A) Magnetic hysteresis loops determined from VSM measurements for magnetite nanoparticles prepared at pH 11 in the presence of different polycations. B–E) FORC measurements of large magnetite nanoparticles grown for 24 h in the presence of JR-400 (B), chitosan (C), poly-L-arginine (D), and PDADMAC (E).

nanoparticles and is a measure of the spectrum of fields due to magnetostatic interaction between particles (see Supporting Information). The first feature is a weak density patch confined to the origin of the FORC diagram. It arises from very fine particles in the SP size range. Although seen in all samples its most substantial contribution is found in poly-L-arginine and PDADMAC, as seen in the reversible component of the magnetization in Figure S18 (Supporting Information). Note that this feature is also displaced above the origin in these two samples, as would be expected for SP nanoparticles.[48] The second feature constitutes a central ridge with a coercivity spectrum between

20 and 70 mT with a narrow spread with respect to the interaction field (B_U), indicative of non-interacting stable single domain.[49] The existence of SSD magnetite is further supported by backfield demagnetization with an average remanent coercivity of ca. 32 mT (Figure S19, Supporting Information). Note that poly-L-arginine and PDADMAC show broader remanent coercivity distributions compared to the other two samples. The third feature is seen as a broad density patch with a coercivity spectrum between ca. 15 and 50 mT and an interaction field of ±30 mT. This feature can either arise from the larger particles that exceed the SSD size range (> 75 nm) or from the clustering of SSD particles.[50] The broad distribution of interaction fields is an expression of nucleation and annihilation fields associated with magnetic vortex states. In the case of PDADMAC is seen as two distinct lobes (Figure 5E), which may reflect the compact structure compared to the sub-structure of the other samples. To summarize, it has been demonstrated that all polycations can be utilized for the growth of magnetite nanoparticles, which possess both superparamagnetic and stable single-domain magnetic properties, and some exhibit magnetic vortex structures. The combination of stable single-domain magnetite nanoparticles and their colloidal stability is advantageous for drug-delivery applications, where cargo can furthermore be linked to functional groups introduced in the polycation.

3. Discussion

This manuscript aims to show that the strong polycations chitosan, JR-400, and PDADMAC have a similar effect on the formation of magnetite nanoparticles as the well-studied poly-L-arginine.[41,42] We previously demonstrated that the addition of poly-L-arginine to the coprecipitation of ferrous and ferric chloride stabilizes amorphous ferrihydrite nanoclusters with a size of 6 nm from which magnetite nanoparticles form through a kinetically controlled monomer addition mechanism.[28] This stabilization, reminiscent of formation pathways of biogenic magnetite, resulted in excellent control over nanoparticle size and shape at ambient conditions. Such improved control, compared to pure magnetite nanoparticles, is likewise achieved through the addition of all polycations tested here.

The first obvious effect of poly-L-arginine on magnetite formation is an inversion of the pH dependence of the nanoparticle size. While magnetite nanoparticles in the absence of additives grow progressively slower at increased alkalinity, the opposite is observed when polycations are present: nanoparticles grow faster at increased pH. This inversion of nanoparticle growth kinetics compared to pure magnetite highlights the polycation's strong influence on the magnetite formation mechanism. Indeed, this effect of pH-dependent nanoparticle size is observed for all polycations tested. It is a direct result of the above-mentioned stabilization of a nanoscopic ferrihydrite precursor from which the magnetite nanoparticles grow via monomer attachment. The attachment reaction follows a base-catalyzed condensation

(oxolation) reaction between the ferrihydrite precursor and the growing magnetite, resulting in an acceleration of the kinetically controlled growth with increasing pH. This stands in contrast to pure magnetite, which exhibits slower growth at increased pH due to a lowering of the magnetite-water surface tension, which favors the formation of smaller magnetite nanoparticles.[6,42,51,52] The observed effect on the dependence of pH on nanoparticle size strongly suggests that magnetite nanoparticles grow by a similar formation mechanism in the presence of polycations. We draw a further analogy in the formation mechanism from the change in nanoparticle morphology, observing solid nanoparticles at pH 9 and 10 and sub-structured single crystals at pH 11. The formation of the latter can be explained by the interaction of the amorphous ferrihydrite precursors with the growing magnetite nanoparticles: On the increase of the pH, the surfaces of magnetite and ferrihydrite become more negative due to the deprotonation of hydroxyl groups. This leads to an increase in the magnetite/ferrihydrite surface tension, and thus a dewetting of the precursor nanoparticles from the magnetite surface. Due to a fast crystallization of ferrihydrite to magnetite at pH 11, the precursor particles crystallize to magnetite before they can sufficiently cover the nanoparticle surface, resulting in a "freezing" of these thermodynamically unfavored structures. In combination with the predicted homoepitaxial crystallization of ferrihydrite onto magnetite, we explain the observed sub-structured but single-crystalline magnetite nanoparticle morphology. Such a rare morphology, observed for poly-L-arginine and sugar-based polycations, further indicates a commonality of the effect of polycations on magnetite formation.

Further evidence for a common formation mechanism for the polycations tested can be drawn from their growth exponents, α, determined by PXRD (Figure 4 and Figures S11–S15, Supporting Information). While pure magnetite exhibits a growth exponent of 1, it increases to 2.6 in the case of poly-L-arginine. This increase, corresponding to a slower growth mechanism, is observed similarly for other polycations that exhibit growth exponents of $\alpha = 4.2$. Such a "slowing down" in the growth mechanism in combination with the observed change in nanoparticle morphology and the dependence on precipitation pH strongly suggests a consistent influence of all polycations on the formation of magnetite. We thus predict that all exhibit the same effect as poly-L-arginine, in that they electrostatically stabilize a transient amorphous ferrihydrite precursor and thus alter the energetic landscape of the formation of magnetite in as is only observed in this sample similar fashion.

We demonstrate above how morphology and size are controlled by the precipitation pH. In the following, we discuss a difference in nanoparticle size as a difference in formation kinetics, since we could show above that larger nanoparticles are formed through faster growth kinetics. While the pH has a well-established effect on the formation kinetics, further control is exerted through the choice of polymer and polymer properties to increase the versatility of the outcome of the synthesis. The influence of the polycations can be thus inferred from their effect on nanoparticle size as a function of pH, varying from poly-L-arginine (12.5 nm pH^{-1}) to the sugar-based polycations chitosan and JR-400 (8.5 nm pH^{-1}). PDADMAC, as an exception, does not exhibit a linear dependency of nanoparticle size with pH suggesting that the presence of PDADMAC suppresses the effect of pH. This likely arises from the strength of the interaction of the polycation with the negatively charged ferrihydrite precursor. In view of the fact that the polycation adsorbed to ferrihydrite is likely not fully integrated into the magnetite crystal lattice, its necessary desorption will influence the kinetics of nanoparticle growth. A slower formation kinetics can thus be deduced from stronger adsorption of the polycations onto the negatively charged precursors, explaining the observed decrease in nanoparticle size dependence on pH (poly-L-arginine < chitosan ≈ JR-400 < PDADMAC). The strong effect, in the case of PDADMAC, can explain the formation of compact nanoparticles, showing no sign of substructuring even at pH 11. The slower formation kinetics may give sufficient time for the amorphous precursors to interact with the magnetite surface. Thus, instead of "freezing" the reaction in a thermodynamically unfavoured morphology during crystallization, as observed for the other polycations, the presence of PDADMAC induces enough time for the formation of thermodynamically favored, solid nanoparticles.

The proposed difference in desorption strength can arise from a variety of difficult-to-entangle structural polymer properties such as intrinsic and electrostatic persistence length, charge density, conformational freedom (and existence) of charged side chains, and the polycation's tendency to condense counter-ions. The quantification of the concerted effect of these parameters on the polymer desorption from ferrihydrite, especially due to its nanoscale curvature, is challenging. Furthermore, the presence of oxygen in all polycations, except for PDADMAC, will have an additional effect, as it is assumed to interact with ferrihydrite. In turn, we can show that a pure polycation, without further functional groups as in the case of PDADMAC, is sufficient to induce biomineralization-reminiscent pathways in magnetite. The surprising ability to obtain large nanoparticles even at pH 9 in the case of PDADMAC highlights how magnetite growth can be accelerated by tuning polycation parameters even at only mildly alkaline conditions, where growth kinetics is expected to be very slow. Such faster growth may indicate how polymer properties can accelerate growth kinetics and may offer an approach to understanding the growth of large magnetosomes in magnetotactic bacteria at very low alkalinity. Our research thus highlights the necessity to further study the effect of polycations in a parameterized approach on the formation of magnetite nanoparticles to understand how crystal growth pathways can be guided by merely changing the composition of the organics involved in the process of biomineralization.

4. Conclusion

In conclusion, we demonstrate how exceptional control over size, size distribution, and dispersibility of magnetite nanoparticles is obtained under ambient conditions by adding strong, pH-independently charged polycations. While the presented research is inspired by the formation of magnetite nanoparticles in magnetotactic bacteria, and biomimetic approaches for magnetite formation have employed expensive and difficult-to-synthesize proteins[35] and proteins analogues[41] limiting scalability, we demonstrate how biomineralization-reminiscent formation pathways can be induced by simple, inexpensive and high yield commercial polycations. We used PDADMAC, a commonly used and simple polycation, as well as sugar-based

polycations, which are sustainably produced from natural resources like shrimp waste (chitosan), or cellulose, which is produced at metric ton scale (under the name JR-400), to obtain improved control over magnetite synthesis under ambient, sustainable conditions. The observed pH-dependent nanoparticle size and morphology, as well as the growth behavior of polycation-containing magnetite nanoparticles, can be compared to the well-understood formation mechanism of magnetite in the presence of another polycation: poly-L-arginine. We can thus generalize that the addition induces the kinetic stabilization of an amorphous ferrihydrite precursor, resembling the formation of magnetite in magnetotactic bacteria. We further show that the possible incorporation of the organic polymer into the inorganic magnetite crystal lattice can alter the magnetic properties of the nanoparticles. The observed deviations for PDADMAC from the reference system containing poly-L-arginine further emphasize the effect of polycation properties including effective charge density and persistence length. A more consistent study of these parameters will advance our current tools for designing synthetic nanoparticles and further our understanding of the effect of macromolecules in the biomineralization of magnetite.

Supporting Information

Supporting Information is available from the Wiley Online Library or from the author.

Acknowledgements

The authors thank Jens Baumgartner and Daniel Chevrier for discussions. MPIKG and HZB are thanked for the allocation of beamtime at the muSpot beamline under proposal number 191-08274-CR. This project was supported by the Max Planck Society and the DFG within the ERA-Chemistry Framework (Project FA 835/12-1). L.K. thanks the Minerva Stiftung for financial support. D.F. is supported by the PTC-MP programm of the CEA (Project HTTPMAGNET).

Conflict of Interest

The authors declare no conflict of interest.

Data Availability Statement

The data that support the findings of this study are available in the supplementary material of this article.

Keywords

bioinspiration, biomineralization, magnetite, non-classical nucleation, sustainability

Received: September 27, 2023
Revised: November 24, 2023
Published online: January 4, 2024

[1] U. Schwertmann, R. Cornell, *The Iron Oxides*, Wiley-VCH, Weinheim, Germany **2004**.
[2] S. Laurent, D. Forge, M. Port, A. Roch, C. Robic, L. Vander Elst, R. N. Muller, *Chem. Rev.* **2008**, *108*, 2064.
[3] S. Staniland, W. Williams, N. Telling, G. Van Der Laan, A. Harrison, B. Ward, *Nat. Nanotechnol.* **2008**, *3*, 158.
[4] S. Kundu, A. A. Kale, A. G. Banpurkar, G. R. Kulkarni, S. B. Ogale, *Biomaterials* **2009**, *30*, 4211.
[5] I. Nyirö-Kósa, A. Rečnik, M. Pósfai, *J. Nanopart. Res.* **2012**, *14*, 10.
[6] J. Baumgartner, L. Bertinetti, M. Widdrat, A. M. Hirt, D. Faivre, *PLoS One* **2013**, *8*, 1.
[7] G. Sherwood, *Mineralogical Magazine* **2002**, *66*, 232.
[8] L. Paltrinieri, M. Wang, S. Sachdeva, N. A. Besseling, E. J. Sudhölter, L. C. De Smet, *J. Mater. Chem. A* **2017**, *5*, 18476.
[9] D. S. Kolchanov, V. Slabov, K. Keller, E. Sergeeva, M. V. Zhukov, A. S. Drozdov, A. V. Vinogradov, *J. Mater. Chem. C* **2019**, *7*, 6426.
[10] H. Zeng, J. Li, J. P. Liu, Z. L. Wang, S. Sun, *Nature* **2002**, *420*, 395.
[11] Y. Sahoo, A. Goodarzi, M. T. Swihart, T. Y. Ohulchanskyy, N. Kaur, E. P. Furlani, P. N. Prasad, *J. Phys. Chem. B* **2005**, *109*, 3879.
[12] M. Lewin, N. Carlesso, C. H. Tung, X. W. Tang, D. Cory, D. T. Scadden, R. Weissleder, *Nat. Biotechnol.* **2000**, *18*, 410.
[13] S. Laurent, S. Dutz, U. O. Häfeli, M. Mahmoudi, *Adv. Colloid Interface Sci.* **2011**, *166*, 8.
[14] S. Sun, H. Zeng, *J. Am. Chem. Soc.* **2002**, *124*, 8204.
[15] D. Kim, N. Lee, M. Park, B. H. Kim, K. An, T. Hyeon, *J. Am. Chem. Soc.* **2009**, *131*, 454.
[16] G. Mirabello, J. J. Lenders, N. A. Sommerdijk, *Chem. Soc. Rev.* **2016**, *45*, 5085.
[17] J. Baumgartner, A. Dey, P. H. Bomans, C. Le Coadou, P. Fratzl, N. A. Sommerdijk, D. Faivre, *Nat. Mater.* **2013**, *12*, 310.
[18] J. C. Aphesteguy, G. V. Kurlyandskaya, J. P. De Celis, A. P. Safronov, N. N. Schegoleva, *Mater. Chem. Phys.* **2015**, *161*, 243.
[19] S. Mann, N. H. Sparks, S. B. Couling, M. C. Larcombe, R. B. Frankel, *J. Chem. Soc., Faraday Trans. 1* **1989**, *85*, 3033.
[20] P. U. Gilbert, S. M. Porter, C. Y. Sun, S. Xiao, B. M. Gibson, N. Shenkar, A. H. Knoll, *Proc. Natl. Acad. Sci. USA* **2019**, *116*, 17659.
[21] S. Weiner, J. Mahamid, Y. Politi, Y. Ma, L. Addadi, *Frontiers of Materials Science in China* **2009**, *3*, 104.
[22] H. Cölfen, S. Mann, *Angew. Chem., Int. Ed.* **2003**, *42*, 2350.
[23] R. A. Van Santen, *J. Phys. Chem.* **1984**, *88*, 5768.
[24] M. Albéric, L. Bertinetti, Z. Zou, P. Fratzl, W. Habraken, Y. Politi, *Adv. Sci.* **2018**, *5*, 5.
[25] V. Schoeppler, D. Stier, R. J. Best, C. Song, J. Turner, B. H. Savitzky, C. Ophus, M. A. Marcus, S. Zhao, K. Bustillo, I. Zlotnikov, *Adv. Mater.* **2021**, *33*, 37.
[26] Z. Zou, L. Bertinetti, Y. Politi, P. Fratzl, W. J. Habraken, *Small* **2017**, *13*, 1.
[27] Z. Zou, X. Yang, M. Albéric, T. Heil, Q. Wang, B. Pokroy, Y. Politi, L. Bertinetti, *Adv. Funct. Mater.* **2020**, *30*, 1.
[28] L. Kuhrts, S. Prévost, D. M. Chevrier, P. Pekker, O. Spaeker, M. Egglseder, J. Baumgartner, M. Pósfai, D. Faivre, *J. Am. Chem. Soc.* **2021**, *143*, 10963.
[29] J. L. Kirschvink, M. M. Walker, C. E. Diebel, *Curr. Opin. Neurobiol.* **2001**, *11*, 462.
[30] J. L. Kirschvink, H. A. Lowenstam, *Earth Planet. Sci. Lett.* **1979**, *44*, 193.
[31] L. M. Gordon, D. Joester, *Nature* **2011**, *469*, 194.
[32] J. Baumgartner, G. Morin, N. Menguy, T. P. Gonzalez, M. Widdrat, J. Cosmidis, D. Faivre, *Proc. Natl. Acad. Sci. USA* **2013**, *110*, 14883.
[33] J. J. Lenders, H. R. Zope, A. Yamagishi, P. H. Bomans, A. Arakaki, A. Kros, G. De With, N. A. Sommerdijk, *Adv. Funct. Mater.* **2015**, *25*, 711.
[34] A. Hajdú, E. Illés, E. Tombácz, I. Borbáth, *Colloids and Surfaces A: Physicochemical and Engineering Aspects* **2009**, *347*, 104.

[35] A. E. Rawlings, L. A. Somner, M. Fitzpatrick-Milton, T. P. Roebuck, C. Gwyn, P. Liravi, V. Seville, T. J. Neal, O. O. Mykhaylyk, S. A. Baldwin, S. S. Staniland, *Nat. Commun.* **2019**, *10*, 1.
[36] A. Pohl, F. Berger, R. M. Sullan, C. Valverde-Tercedor, K. Freindl, N. Spiridis, C. T. Lefèvre, N. Menguy, S. Klumpp, K. G. Blank, D. Faivre, *Nano Lett.* **2019**, *19*, 8207.
[37] C. L. Altan, B. Gurten, R. Sadza, E. Yenigul, N. A. Sommerdijk, S. Bucak, *J. Magn. Magn. Mater.* **2016**, *416*, 366.
[38] S. Si, A. Kotal, T. K. Mandal, S. Giri, H. Nakamura, T. Kohara, *Chem. Mater.* **2004**, *16*, 3489.
[39] G. Mirabello, A. Keizer, P. H. Bomans, A. Kovács, R. E. Dunin-Borkowski, N. A. Sommerdijk, H. Friedrich, *Chem. Mater.* **2019**, *31*, 7320.
[40] A. Arakaki, F. Masuda, Y. Amemiya, T. Tanaka, T. Matsunaga, *J. Colloid Interface Sci.* **2010**, *343*, 65.
[41] J. Baumgartner, M. Antonietta Carillo, K. M. Eckes, P. Werner, D. Faivre, *Langmuir* **2014**, *30*, 2129.
[42] L. Kuhrts, E. Macías-Sánchez, N. V. N. Tarakina, A. M. A. Hirt, D. Faivre, *J. Phys. Chem. Lett.* **2019**, *10*, 5514.
[43] V. Reichel, A. Kovács, M. Kumari, É. Bereczk-Tompa, E. Schneck, P. Diehle, M. Pósfai, A. M. Hirt, M. Duchamp, R. E. Dunin-Borkowski, D. Faivre, *Sci. Rep.* **2017**, *7*, 1.
[44] J. I. Langford, A. J. C. Wilson, *J. Appl. Crystallogr.* **1978**, *11*, 102.
[45] A. Fischer, M. Schmitz, B. Aichmayer, P. Fratzl, D. Faivre, *J. R. Soc., Interface* **2011**, *8*, 1011.
[46] B. Pokroy, A. N. Fitch, F. Marin, M. Kapon, N. Adir, E. Zolotoyabko, *J. Struct. Biol.* **2006**, *155*, 96.
[47] A. Lang, I. Polishchuk, E. Seknazi, J. Feldmann, A. Katsman, B. Pokroy, *Adv. Funct. Mater.* **2020**, *30*, 1.
[48] R. Pike, *Phys. Rev. B: Condens. Matter Mater. Phys.* **2003**, *68*, 104424.
[49] R. Egli, A. P. Chen, M. Winklhofer, K. P. Kodama, C.-S. Horng, *Phys. Rev. B: Condens. Matter Mater. Phys.* **2010**, *11*, Q01Z11.
[50] A. P. Roberts, T. P. Almeida, N. S. Church, R. J. Harrison, D. Heslop, Y. Li, J. Li, A. R. Muxworthy, W. Williams, X. Zhao, *Journal of Geophysical Research: Solid Earth* **2017**, *122*, 9534.
[51] J. P. Jolivet, C. Froidefond, A. Pottier, C. Chanéac, S. Cassaignon, E. Tronc, P. Euzen, *J. Mater. Chem.* **2004**, *14*, 3281.
[52] L. Vayssieres, *Int. J. Nanotechnol.* **2005**, *2*, 411.